Theses and Dissertations   Student Graduate Works

3-14-2014

Direct Emissivity Measurements of Painted Metals for Improved Temperature Estimation During Laser Damage Testing

Sean M. Baumann

Follow this and additional works at: https://scholar.afit.edu/etd

Part of the Optics Commons

DIRECT EMISSIVITY MEASUREMENTS OF PAINTED METALS

FOR IMPROVED TEMPERATURE ESTIMATION DURING

LASER DAMAGE TESTING

THESIS

Sean M. Baumann, Civilian

AFIT-ENP-14-M-43

DEPARTMENT OF THE AIR FORCE
AIR UNIVERSITY

AIR FORCE INSTITUTE OF TECHNOLOGY

Wright-Patterson Air Force Base, Ohio

The views expressed in this thesis are those of the author and do not reflect the official policy or position of the United States Air Force, the Department of Defense, or the United States Government.

This material is declared a work of the U.S. Government and is not subject to copyright protection in the United States.

AFIT-ENP-14-M-43

DIRECT EMISSIVITY MEASUREMENTS OF PAINTED METALS

FOR IMPROVED TEMPERATURE ESTIMATION DURING

LASER DAMAGE TESTING

THESIS

Presented to the Faculty

Department of Engineering Physics

Graduate School of Engineering and Management

Air Force Institute of Technology

Air University

Air Education and Training Command

in Partial Fulfillment of the Requirements for the

Degree of Master of Science in Optical Science and Engineering

Sean M. Baumann, B.A.

Civilian

March 2014

DISTRIBUTION STATEMENT A:
APPROVED FOR PUBLIC RELEASE; DISTRIBUTION UNLIMITED

DIRECT EMISSIVITY MEASUREMENTS OF PAINTED METALS

FOR IMPROVED TEMPERATURE ESTIMATION DURING

LASER DAMAGE TESTING

Sean M. Baumann, B.A.
Civilian

Approved:

//signed//	17 March 2014
Michael A. Marciniak, PhD (Chairman)	Date

//signed//	17 March 2014
Glen P. Perram, PhD (Member)	Date

//signed//	17 March 2014
Christopher A. Rice, PhD (Member)	Date

Abstract

A database of spectral, temperature dependent emissivities was created for a range of painted aluminum laser damage testing targets with the purpose of improving accuracy in temperature estimates on front and back target surfaces during laser damage tests. Previous temperature estimations were made by fitting an assumed graybody radiance curve to the radiance measured from the back surface via a Telops imaging Fourier transform spectrometer. In this work, spectral emissivity measurements were made using an SOC-100 hemispherical directional reflectometer and Nicolet Fourier transform infrared spectrometer. Of particular interest was a high temperature matte black enamel paint used to coat the rear surfaces of the aluminum samples. Previously, the paint was assumed to have a spectrally flat and temperature-invariant emissivity. Collected data showed spectral variance and temperature dependence. Back-surface temperature estimations of laser damage test samples were improved from $\pm 25°$ C to $\pm 5°$ C away from the beam center. At beam center, temperatures exceeded the capabilities of the reflectometer, so a new method was developed using a mid-infrared laser probe to measure temperature dependent reflectance. The new method may be used in future laser damage tests to estimate single-wavelength temperatures up to the target melting point. Accurate temperature measurements in laser damage testing will be helpful in informing a predictive model for future high energy laser weapon engagements.

For my family

Acknowledgments

Sean M. Baumann

Table of Contents

List of Figures

List of Symbols

Symbol	Definition
L_e	Radiance ($W/cm^2\ sr\ \mu m$)
M_e	Radiant Exitance (W/cm^2)
E_e	Irradiance (W/cm^2)
Ω	Solid angle (sr)
FFT	Fast fourier transform
V	voltage (volts)
α	absorptance
ρ	reflectance
τ	transmittance

Subscripts

bb	black body
sam	sample
ref	reference
s	source
t	target
B	brightness temperature
i	incident
r	reflected
RT	room temperature

List of Acronyms

Acronym	Definition
HEL	High Energy Laser
LWIR	Long Wave Infrared
MWIR	Mid Wave Infrared
NIR	Near Infrared
LHMEL	Laser Hardened Materials Evaluation Laboratory
IFTS	Imaging Fourier Transform Spectrometer
HDR	Hemispherical Directional Reflectance
DHR	Directional Hemispherical Reflectance
FTIR	Fourier Transform Infrared
KBr	Potassium Bromide
DTGS	Doped Triglycine Sulfate
FFT	Fast Fourier Transform
InSb	Indium Antimonide
PID	Proportional-integral-derivative
RT	room temperature
OAP	off-axis parabolic mirror
NET	noise-equivalent temperature

DIRECT EMISSIVITY MEASUREMENTS OF PAINTED METALS FOR IMPROVED TEMPERATURE ESTIMATION DURING LASER DAMAGE TESTING

I.   Introduction

1.1   Motivation

The laser first became a presence on the battlefield during the Vietnam War, when the U.S. Air Force introduced the Paveway series of laser-guided bombs. While these laser-guided munitions were state of the art at the time, development of the laser as a directed energy weapon has continued to the point where High Energy Laser (HEL) weapons must be studied in terms of their predicted effect upon interaction with a target. These laser-target interactions are driven by a wide variety of factors, including the laser's chosen gain medium and wavelength, overall laser power, beam diameter, atmospheric influences, and target composition.

When considering target composition, one of the likely engagement scenarios for an HEL weapon will be with a painted metal object. In this case, knowledge of both the paint and metal substrate will help predict the effectiveness of the weapon. However, because both the paint and the metal change during the engagement, more work must be done to better understand the target's changing characteristics as it is affected by directed energy from the weapon system.

1.2   Previous Research

Studies of laser damage on painted metals have occurred since the 1970's [1], when the most common kilowatt-class laser available was a Long Wave Infrared (LWIR) CO_2

1

laser operating at 10.6 μm. These tests first established the importance of the paint coating as an absorptive coupler of energy into the metal, and established a paint-residue model to predict absorptance as functions of irradiance and paint thickness [2].

However, as the technology has matured, HEL weapons have transitioned into the Near Infrared (NIR) (0.7-3 μm) regime. These wavelengths are the focus of current military research due to the fact that, in part, shorter wavelength lasers have better divergence characteristics and are more efficient. At NIR wavelengths, the color and composition of the paint coatings on the target become more important.

Recent high energy laser damage tests conducted at the Laser Hardened Materials Evaluation Laboratory (LHMEL) have sought to achieve greater understanding of how variables such as coating composition, target environment and irradiance level affect the laser damage mechanisms. During these tests, temperature measurements of the rear surface of the laser damage samples were attempted via thermocouple. It was assumed that after the laser damage test sample was penetrated, the thermocouple would melt almost immediately. However, it was discovered that the thermocouple took up to a second or more to melt, rendering its temperature measurements unusable. Later tests attempted to measure back surface temperature using a Telops Imaging Fourier Transform Spectrometer (IFTS) sensitive in the Mid Wave Infrared (MWIR) observing thermal emission from a high-emissivity coating on the rear surface. Accurate rear-surface temperature data and burn-through times are of great importance for the development of a heat-transfer model to predict burn-through times over a wide range of real-world engagement scenarios.

1.3 Objectives

Uncertainty from the IFTS data on back-surface temperature during laser-damage testing led to questions regarding the previous assumptions that the emissive coating on the back surface of the samples was spectrally uniform, as well as whether its emissivity

2

changes as the sample is heated to melt temperature. To answer these questions, the following objectives were developed:

1. Make detailed measurements of spectral emissivities of the samples as they are heated to melt temperature and compare the temperature uncertainties inferred from this data with those made assuming a graybody emissivity.

2. If a strong temperature-dependence is found, develop a method for real-time *in situ* emissivity measurement via laser reflectance probe.

1.4 Thesis Overview

The following chapters will detail the research performed for this thesis step-by-step, organized as follows:

- **Chapter II** - A review of the basic theoretical concepts to be applied in the investigation of both objectives.

- **Chapter III** - Description of the equipment and methods used to establish the emissivity database.

- **Chapter IV** - Presentation of results from Objective 1, and a discussion of the value and limitations of the spectral emissivity values.

- **Chapter V** - Description of the equipment and methods used to address Objective 2

- **Chapter VI** - Presentation of the results of the second experiment, and an analysis of the generated data and its applicability to future laser damage tests

- **Chapter VII** - Summary of the contributions of this research and recommendations for future research.

3

II.   Theoretical Background

2.1   Emissivity Database

An understanding of the work presented in this thesis is incomplete without knowledge of radiometry and its associated quantities, blackbody radiation theory, and hemispherical directional reflectance. This chapter will familiarize the reader with these concepts as they pertain to the first objective of creating a temperature-dependent, spectral emissivity database

2.1.1   Basics of Radiometry.

Radiometry is described as "the measurement of optical radiant energy."[3] These measurements stem from a few fundamental quantities, listed with their units and descriptions here:

2.1.2   Radiance and Solid Angle.

Radiance (L_e) is the elemental quantity of radiometry. It describes the total radiant flux (Φ_e), per unit area (A), per unit projected solid angle (Ω). In SI units, it is presented in units of $W/cm^2\,sr$, or when considering spectral radiance, in $W/(cm^2\,sr\,\mu m)$. Of note is the unit of solid angle, sr, known as a steradian. One steradian is defined as the solid angle that, having its vertex in the center of a sphere, cuts off an area of the surface of the sphere, A, equal to that of a square with sides of length equal to the radius, r, of the sphere [4]. Its definition is

$$\Omega = \frac{A}{r^2}. \tag{2.1}$$

Radiance can be related to the total optical power in a system (in Watts, W) through (2.2), where A_s is the projected area of the radiation source and Ω is the projected solid angle into which the radiance is emitted, most often subtended by a detector.

4

$$\Phi = \iint L_e \, dA_s \, d\Omega \qquad (2.2)$$

2.1.3   Exitance and Irradiance.

These two radiometric quantities, exitance, M_e, and irradiance, E_e, are expressed in the same units (W/cm^2) but describe two different geometries. Exitance describes radiation that exits a source into a full hemisphere, while irradiance describes the total power per unit area (A_t) incident onto a surface. Exitance and Irradiance are expressed mathematically as (2.3), and (2.4), respectively.

$$M_e = \frac{\partial \Phi_e}{\partial A_s} \qquad (2.3)$$

$$E_e = \frac{\partial \Phi_e}{\partial A_t} \qquad (2.4)$$

2.1.4   Blackbody Radiation Theory.

Thermal sources of optical radiation have been studied since the late nineteenth century. Early on, it was known that the total radiated power was proportional to the temperature of the source. The Stefan-Boltzmann Law (2.5), formulated in 1884, predicts the total radiant exitance of a source given a temperature, T,

$$M_e(T) = \sigma T^4, \qquad (2.5)$$

where $\sigma = 5.67 * 10^{-8} \ W/\left(m^2 K^4\right)$. This equation (2.5) describes the behavior of a blackbody, an idealized object that absorbs all light incident upon it and is a perfect emitter of thermal radiation at a given temperature. While a blackbody's total radiant exitance had been described by the Stefan-Boltzmann law, it wasn't until 1901 when the spectrally-defined blackbody radiance equation was developed,

$$L_{bb}(\lambda, T) = \frac{2hc^2}{\lambda^5(e^{hc/(\lambda k_b T)} - 1)}, \qquad (2.6)$$

where h is Planck's constant, c is the speed of light in a vacuum, k_b is Boltzmann's constant, λ is the emitted wavelength, and T is the temperature in Kelvin. Figure 2.1 shows the

5

spectral radiance profiles as predicted by Planck's equation, across a range of temperatures applicable to laser damage testing.
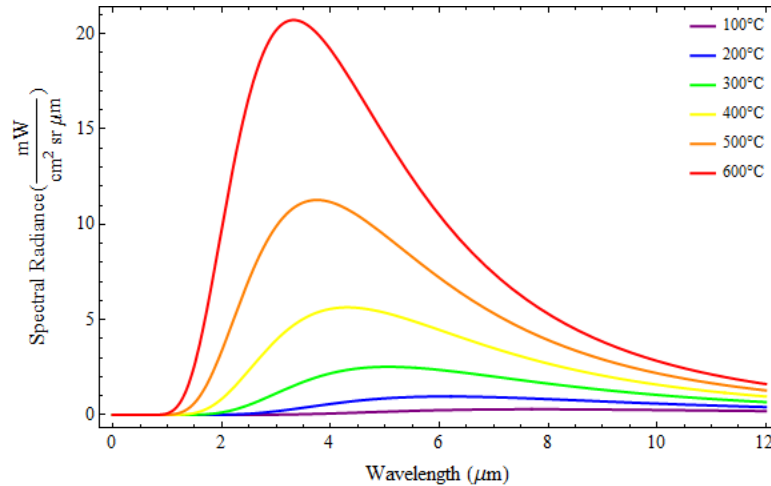
Figure 2.1: Blackbody spectral radiance curves for temperatures from 100° C to 600° C.

As an ideal blackbody is a perfect absorber and emitter, it is used as a standard by which real-world materials are measured in their interaction with radiant energy. These measured quantities, and their descriptions, follow.

2.1.5   Reflectance and Absorptance.

When radiant energy is incident on a material, the law of conservation of energy dictates that the radiation be either absorbed, reflected or transmitted. The characteristics of how a material interacts with radiant energy are described by its absorptance (α), reflectance (ρ), and transmittance (τ). Each value describes the fraction of incident radiant energy that is absorbed, reflected, and transmitted. All three values must together sum to the total amount of incident energy, as prescribed in

$$\alpha + \rho + \tau = 1, \tag{2.7}$$

where α is absorptance, ρ is reflectance, and τ is transmittance. Due to the opaque nature of the painted metal samples being studied, the assumption is made here that $\tau = 0$.

6

In real materials, these quantities are dependent on wavelength (λ), incident angle of the incoming radiation (θ), and the temperature of the material (T). Therefore, a more general equation for the relationship between reflectance and absorptance is

$$\rho(\lambda, \theta, T) + \alpha(\lambda, \theta, T) = 1. \tag{2.8}$$

2.1.6 Kirchoff's Law and Emissivity.

Kirchoff's Law dictates that at thermal equilibrium, the radiant energy emitted by a material must equal the radiant energy absorbed by it, such that

$$\alpha(\lambda, \theta, T) = \epsilon(\lambda, \theta, T), \tag{2.9}$$

where ϵ is emissivity. This material property is of great importance when describing the radiant thermal energy from a source. This value will effectively scale down the blackbody radiance curve at a given temperature. A definition of emissivity from *The Infrared Handbook* [5] in terms of the material radiance is given in (2.10)

$$\epsilon(\lambda, \theta, T) = \frac{L_e(\lambda, \theta, T)}{L_{bb}(\lambda, T)} \tag{2.10}$$

where L_e is the emitted spectral radiance of the material in question and L_{bb} is the ideal blackbody spectral radiance. When $\epsilon = 1$, the object is considered a blackbody. When ϵ takes some constant value, with respect to wavelength, between 0 and 1 (i.e. $\epsilon \neq f(\lambda)$), it is considered a *graybody*. However, most real-world objects have a wavelength-dependence and are known as *selective emitters*, or *selective radiators*. Comparisons of the three cases are shown in Figure 2.2:

7
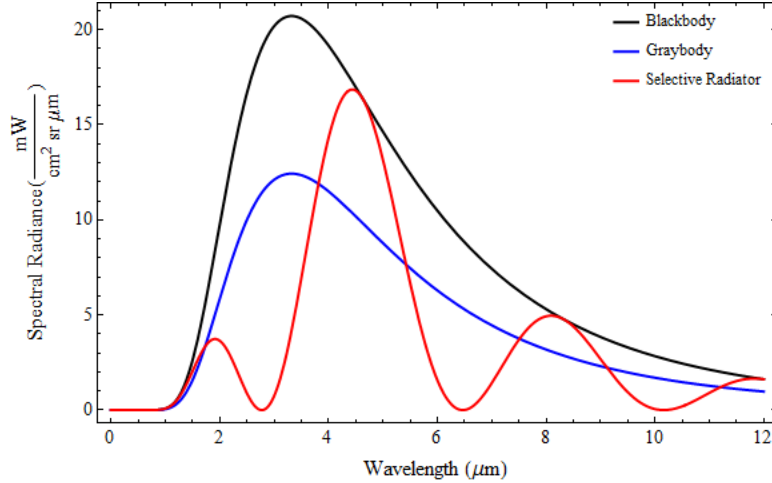
Figure 2.2: Spectral radiance curves of a perfect blackbody, a graybody ($\epsilon = 0.6$), and a selective emitter ($\epsilon = f(\lambda)$).

2.1.7 Radiometric Temperature Measurement.

Modern spectrometers allow for accurate radiance measurements with fine spectral resolution. Following proper calibration and correction for atmospheric transmittance (τ_{atm}), equation (2.11) can be worked to solve for an object temperature, given a known object emissivity and measured radiance.

$$L_{meas}(\lambda) = \epsilon(\lambda)\tau_{atm}(\lambda)\frac{2hc^2}{\lambda^5(e^{hc/\lambda k_b T} - 1)} \tag{2.11}$$

In recent laser damage tests where back-surface temperature was estimated, a high-temperature matte black paint was applied to the back surface of the samples. The paint was assumed to have a spectrally flat emissivity of approximately 0.95. However, temperature estimations resulting from the assumed emissivity had large uncertainties ($\pm 25°$ C), so the need arose to empirically measure the spectral emissivities of these paints.

2.1.8 Directional Reflectance Measurement.

During the previous discussion of absorptance, reflectance, and emissivity, relationships were established between the three that enable a material's emissivity to be measured

8

from its reflectance. When equation (2.9) is substituted into (2.7) and solved for ϵ, (2.12) establishes the relationship that allows emissivity to be inferred from reflectance.

$$\epsilon(\lambda, \theta, T) = 1 - \rho(\lambda, \theta, T) \tag{2.12}$$

Measurement of directional reflectance can be conducted one of two ways: Directional Hemispherical Reflectance (DHR) or Hemispherical Directional Reflectance (HDR), diagrammed in Figure 2.3. [6] In DHR measurements (Fig 2.3a), a sample is illuminated from a single, variable direction and all reflected radiation is measured. The reciprocal of this technique is HDR, in which the sample, located at one focal point of a hemi-ellipsoidal mirror, is illuminated by a blackbody source located at the other focal point of the mirror. The reflected radiance is then sampled from one direction. Because previous laser damage tests had observed the radiance pattern from the back surface at near-normal angles, the reflectances, and by derivation, the emissivities, of these samples will be measured near-normal as well.

9

| (a) DHR | (b) HDR |
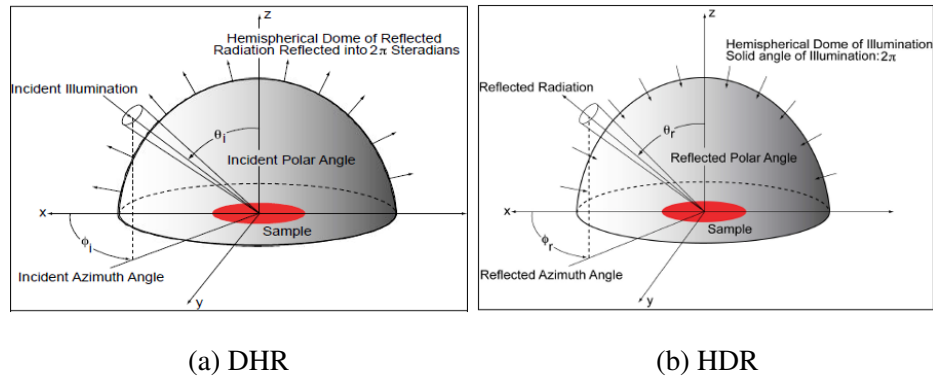
Figure 2.3: Comparison between two directional reflectance measurement methods. The DHR method (2.3a) involves incident light from a single angle being collected over its entire hemisphere after reflection. The HDR method (2.3b) involves incident light from all directions collected at a single reflected direction. [6] (Reprinted with permission from the authors)

2.2 Laser Reflectance Probe

This section of background theory will focus on the principles behind the implementation of a laser reflectance probe to estimate target back surface temperatures from single wavelength radiance during future laser damage tests. Topics will include the details of optical reflectance spectroscopy, obtaining an accurate temperature estimation from single wavelength reflectance and radiance data, and the principles behind extracting modulated data from high-noise backgrounds.

2.2.1 Optical Reflectance Thermometry.

Optical reflectance thermometry is a technique whereby a temperature can be inferred by measuring a change in reflectance, at a single wavelength, from a laser beam incident on the surface in question. [7] When a material undergoes a change in temperature, ΔT, its reflectance undergoes a corresponding change. In general, the formula relating reflectance

10

change to temperature change is given by Claeys *et al*; as

$$\rho(T(t)) = \rho_0 + \frac{\delta\rho}{\delta T}(T_0 + \Delta T) \tag{2.13}$$

where T_0 is the starting temperature, and ρ_0 is the material's reflectance at room temperature. The quantity $\delta\rho/\delta T$ refers to the material's previously measured, reliable temperature dependence of reflectance at the laser probe's wavelength. [8]

Laser-probe-based temperature estimations have been reliably made in the past. Lee and Norris demonstrated a technique for measuring temperatures on solid surfaces via laser reflectance at high incident angles. [7] Accurate temperature measurements have also been made at liquid surfaces by Longtin and Fan. [9] The technique has value in its ability to acquire data quickly, in that it does not require a thermocouple to be placed in a destructive environment, and in that it is capable of high temporal resolution.

Most techniques for optical reflectance thermometry involve measuring specular reflectance. Specular reflectance refers to the classical case where the law of reflection applies, namely that the angle of the incident beam relative to the surface's normal will be the same as the angle of the reflected beam, so $\theta_i = \theta_r$. Diffuse reflectance, on the other hand, refers to light that reflects into any other direction off of the surface in question. The chosen incidence angle has varied significantly depending on the application. Longtin *et al.* used an incident angle of near normal in their measurement of liquid temperature due to the greater relative changes in signal between temperatures. [9] Iuchi and Wada, by comparison, probed their metal samples at an $80°$ incident angle because the total reflected signal is highest at grazing angles. [10]

2.2.2 *Single-Wavelength Temperature Estimation.*

Given a spectral radiance as shown in (2.11), there are several ways to estimate a material's temperature. Among them is *brightness temperature* which is defined as the temperature of a blackbody that gives the same radiance in a narrow spectral region about a central wavelength, λ_0, as the radiance measured for a source at λ_0. [11] In the case

11

where emissivity is unknown, $\epsilon(\lambda_0)$ is assumed to be 1 and brightness temperature is an approximation. However, when emissivity at the chosen wavelength, λ_0, is known, the brightness temperature equals the true temperature. Equation (2.14) shows the spectral radiance equation for a narrow waveband about a single wavelength, λ_0, its approximation in terms of brightness temperature (T_B), and its exact quantity in terms of spectral emissivity ($\epsilon(\lambda_0)$) and true temperature (T).

$$L(\lambda_0) = \frac{2hc^2}{\lambda_0^5(e^{hc/\lambda_0 k_b T_B} - 1)} = \epsilon(\lambda_0)\frac{2hc^2}{\lambda_0^5(e^{hc/\lambda_0 k_b T} - 1)} \tag{2.14}$$

After solving (2.14) for true temperature, T, in terms of the collected radiance, the equation for temperature is found directly.

$$T = \frac{hc}{k_b\lambda_0} \cdot \ln^{-1}\left(\frac{2\epsilon_\lambda hc^2}{L(\lambda_0)\lambda_0^5} + 1\right) \tag{2.15}$$

2.2.3 *Phase-Sensitive Detection and the Lock-In Amplifier.*

Lock-in amplifiers are devices that employ a technique called phase-sensitive detection in order to excise small AC signals from large amounts of noise. [12] The principle relies on the orthogonality of sinusoidal functions at different frequencies. To accomplish this, the lock-in amplifier requires an AC reference to compare to the detected signal. Consider a modulated signal, $V_{sig}\sin\left(\omega_R t + \theta_{sig}\right)$, and a reference signal either generated by, or sent to, the lock-in amplifier. This reference is of the form $V_{ref}\sin\left(\omega_L t + \theta_{ref}\right)$. The lock-in amplifier then multiplies the signal with the reference as shown in equations (2.16).

$$V_{psd} = V_{sig}V_{ref}\sin\left(\omega_R t + \theta_{sig}\right)\sin\left(\omega_L t + \theta_{ref}\right) \tag{2.16a}$$

$$V_{psd} = \frac{1}{2}V_{sig}V_{ref}\cos\left([\omega_R - \omega_L]t + \theta_{sig} - \theta_{ref}\right) - \frac{1}{2}V_{sig}V_{ref}\cos\left([\omega_R + \omega_L]t + \theta_{sig} + \theta ref\right) \tag{2.16b}$$

The resultant signal, V_{psd}, is then sent through a low pass filter, where all AC signals are removed. In the case where the difference between the signal and reference frequencies

12

is 0, the PSD output will be

$$V_{psd} = \frac{1}{2} V_{sig} V_{ref} \cos\left(\theta_{sig} - \theta_{ref}\right). \tag{2.17}$$

Some lock-ins have the ability to alter the reference offset, θ_{ref}, through the use of a second phase-sensitive detector. This second detector (or channel), shown in Equation (2.18), adds a 90° phase shift to the reference.

$$V_{psd2} = \frac{1}{2} V_{sig} V_{ref} \sin\left(\theta_{sig} - \theta_{ref}\right). \tag{2.18}$$

This second channel allows for maximization of the signal by computing the overall magnitude (2.19a) of the signal, and phase (2.19b) between the signal and reference.

$$R = \sqrt{V_{psd}^2 + V_{psd2}^2} \tag{2.19a}$$

$$\theta = \tan^{-1}\left(\frac{V_{psd2}}{V_{psd}}\right) \tag{2.19b}$$

13

2.3 Summary

In this chapter, the theoretical background necessary to understand the two objectives of this research was summarized. The first topics discussed were the basics of radiometry, blackbody radiation theory, the law of conservation of energy and Kirchoff's Law. These topics allow an understanding of the way materials radiate thermal energy and the way a material responds to incident light.

Next, directional reflectance measurement theory was discussed. The two principal methods for measurement were discussed and justification given for the chosen HDR method. This directional reflectance method will be used to derive emissivity through Kirchoff's Law, and with this knowledge, it is hoped that accurate temperature estimations can be made on laser damage test samples.

Finally, the principles of reflectance thermometry were summarized. A laser source may be used to probe the surface of the material to measure a change in reflectance. This value can be used to infer an emissivity, from which a true temperature may be inferred from the single-wavelength temperature estimate. Last, the means for measuring a modulated laser signal with excellent signal to noise was discussed. It is with this knowledge that a detailed discussion of the experimental methods and results may be had.

III. Experimental Method: Emissivity Database

The contents of this chapter describe in detail the laboratory setup, equipment used, and experimental method employed to develop the temperature-dependent emissivity database.

3.1 Measurement Equipment

The emissivity measurements on painted aluminum 2024-T3 alloy samples were performed in an apparatus with two major components: the SOC-100 HDR and a Thermo Scientific Nicolet 6700 Fourier Transform Infrared (FTIR) spectrometer, shown in Figure 3.1.
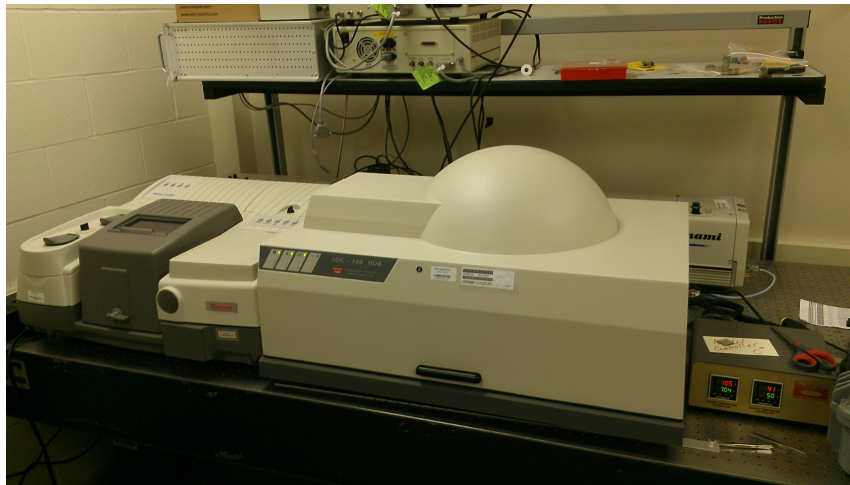
Figure 3.1: SOC-100 HDR (right) with temperature control unit, attached to Thermo Scientific Nicolet 6700 FTIR (left).

3.1.1 SOC-100 HDR.

The SOC-100 is a reflectometer, built by the Surface Optics Corporation in San Diego, CA. Its primary purpose is the measurement of directional reflectance and transmittance.

Of the two methods outlined in Chapter II (DHR and HDR), the SOC-100 utilizes the HDR measurement method by illuminating a sample from all directions above it. A more detailed description of its components, shown in Figure 3.2, follows below.
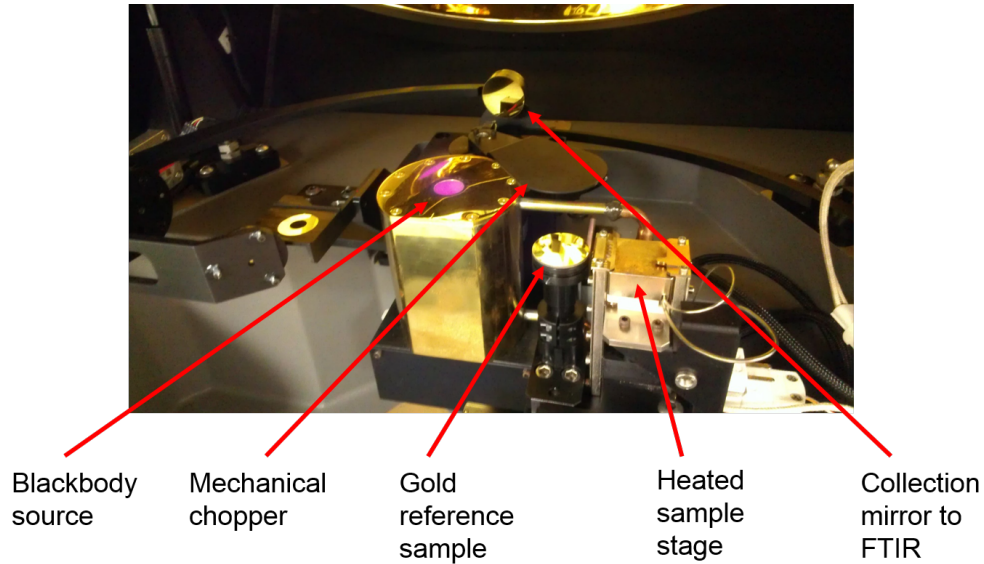
Figure 3.2: SOC-100 internals with hemi-ellipsoidal mirror lifted: blackbody radiation source and mechanical chopper, gold reflectance standard and heated sample stage, and transfer optics

3.1.2 Infrared Radiation Source and Chopper.

The blackbody radiation source is an electrically heated, conical, stainless steel cavity with an oxidized emitting surface to ensure uniform high-emissivity. At the top of the cavity is a 0.75" gold collar, which exists to ensure uniform radiance at angles very close to 90°. The casing of the radiation source is liquid-cooled to ensure no improper heating of the other components within the reflectometer.

Adjacent to the IR radiation source is a mechanical chopper, whose movements are directed by signals from the FTIR. The movements of the chopper allow the FTIR to

www.manaraa.com

collect spectra from the sample both when illuminated by the IR source and when only self-emitting.

3.1.3 Hemi-ellipsoidal Mirror.

The HDR method of measuring directional reflectance relies on the ability of the system to illuminate the sample over its entire 2π steradian upper hemisphere. However, this is not physically realizable, due to the necessary presence of measurement arms. However, this "incomplete hemisphere error" is minimized both by reducing the size of the measurement of the additional overhead optics, and by enlarging the hemi-ellipsoidal mirror relative to the additional optics. The hemi-ellipsoidal mirror inside the SOC-100 has a semimajor axis of 18", and 1.8" foci separation. [6] One complication involved in using a hemi-ellipsoidal mirror is that the re-imaging from object space to image space generates distortions. Figure 3.3 shows this relationship, and the necessity for the sample being measured in the image plane to be larger than the radiation source in the object plane. [13]
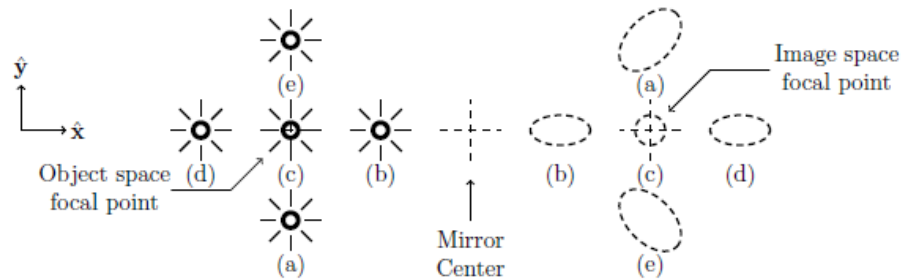
Figure 3.3: Lambertian point sources re-imaged under a hemi-ellipsoidal mirror. Objects at the first focal point are enlarged at the second focal point. (Reprinted with permission from the authors.)

3.1.4 Sample Stage and Gold Reference.

At the second focus of the hemi-ellipsoidal mirror is a translation stage, which can alternate between a specular gold reference standard, and the sample stage. Again, the movement of the sample stage is controlled by computer. The gold reference is measured and compared against its known directional reflectance properties to achieve proper calibration, then the test sample is moved into the second focus to be measured. The sample stage selected for this experiment has the ability to control the sample temperature up to 500° C, and is fitted with a nitrogen gas purge that blows cool nitrogen gas over the sample to prevent overheating from the incident radiant energy.

3.1.5 Transfer Optics.

Reflected radiation from the test sample is collected by a 1" ellipsoidal mirror, able to rotate to any polar angle, in a plane, above the sample. The mirror collects the reflected light from the sample and refocuses it onto a 0.32" diameter aperture, located on the rotation axis of the collection mirror. Beyond the aperture, the light is then reflected from a flat mirror into a 90° off-axis parabolic mirror (OAP), which effectively collimates the light as it exits the reflectometer.

3.1.6 Fourier Transform Spectrometer.

The SOC-100 HDR was designed specifically to mate with a Thermo Scientific Nicolet FTIR, whose internals are shown in Figure 3.4, courtesy of Thermo Electron Corporation. [14] The instrument is equipped with a Potassium Bromide (KBr) beamsplitter, and Doped Triglycine Sulfate (DTGS) detectors, sensitive from 2 to 25 μm. As is typical of an FTIR device, the incoming light from the SOC-100 is passed through a Michelson Interferometer. The Fourier transform of the resulting interferogram is then used to create the reflectance spectrum.

18
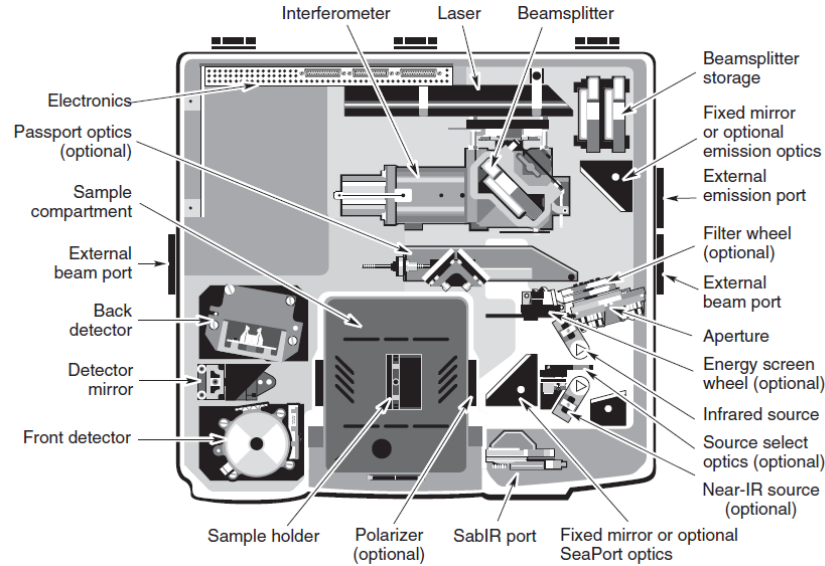
Figure 3.4: Internal Components of the Nicolet Fourier Transform Infrared Spectrometer. (Reprinted with permission from the authors.)

3.2   Methodology

3.2.1   Sample Characteristics.

The primary samples used were aluminum alloy Al2024 T3, a common aircraft structural metal used in many previous laser damage tests. Three coating options were studied. The primary focus of the study was the high-temperature stove black coating applied to the back surfaces of the laser damage samples. However, bare aluminum and a light gray camouflage paint coating were also studied. Each sample was 0.82 mm thick, with paint coating thickness of approximately 50 μm.

3.2.2   Measurement Procedure.

The SOC-100 automates the data collection procedure by operating the shutter over the IR source and translating the sample stage between the gold reference and the test sample. Parameters may be selected to maximize signal and measurement accuracy. All measurements were taken over the 2-12 μm wavelength band with $4\,cm^{-1}$ spectral

resolution, with the collection mirror at 10° from normal, with 20 scans from reference to sample per measurement. Each measurement was performed four times and averaged to give a total spectral reflectance.

The samples were heated in 50° C increments until the heated sample stage reached its maximum set temperature of 500° C. Samples took approximately one minute to reach each temperature, and were maintained at each temperature for ten minutes while the scans were made. After reaching the maximum temperature of 500° C, samples were cooled at 50° C intervals and measurements were collected again until the samples returned to room temperature.

3.2.3   *Calculation of Sample Reflectance and Emissivity.*

Final calculation of the sample's directional reflectance involves four separate measurements, made and stored to the computer automatically, listed below with their abbreviations:

- Interferogram of the reference taken with the chopper open - $I_{ref}^{op}(\lambda)$

- Interferogram of the reference taken with the chopper closed - $I_{ref}^{cl}(\lambda)$

- Interferogram of the sample taken with the chopper open - $I_{sam}^{op}(\lambda)$

- Interferogram of the sample taken with the chopper closed - $I_{sam}^{cl}(\lambda)$

With these four measurements, the computer then performs a Fast Fourier Transform (FFT) on each, and according to Equation (3.1), calculates the sample's spectral reflectance at a given angle, in this case where $\theta = 10°$ to simulate the positioning of the Telops IFTS.

$$\rho_{sam}(\lambda) = \rho_{ref}(\lambda) \cdot \left[\frac{FFT[I_{sam}^{op}(\lambda)] - FFT[I_{sam}^{cl}(\lambda)]}{FFT[I_{ref}^{op}(\lambda)] - FFT[I_{ref}^{cl}(\lambda)]} \right] \tag{3.1}$$

With the spectral reflectance data in hand, the process of converting to emissivity is completed by simply evaluating Equation (2.12) at every measured wavelength.

20

3.3 Summary

This chapter has discussed the equipment and methodology used to create the emissivity database. Samples are placed in a temperature-controlled stage in the SOC-100 HDR, where they are illuminated by an infrared radiation source. The reflected light is collected and analyzed in an FTIR spectrometer. Interferograms from the samples are then compared with those from a gold reference, and reflectance spectra are created, and in turn, converted to emissivity spectra.

IV. Results and Discussion: Emissivity Database

In this chapter, the final development of the temperature-dependent, spectral emissivity database is discussed. The emissivity database is then applied to spectral radiance data of painted metals, collected by the Telops IFTS during previous laser damage tests. The new database will then be evaluated on its ability to accurately predict back-surface temperatures, as compared with previous emissivity models.

4.1 Emissivity Database

Samples from previous laser damage tests were acquired for spectral, temperature-dependent emissivity measurements. The Al2024-T3 samples were studied under three coating scenarios: uncoated, light gray camouflage paint on chrome-based primer, commonly found on the front surface of laser damage test samples, and the back-surface matte black high-emissivity paint. Of particular interest in this experiment was the matte black paint present on the back surfaces of the test samples. Each sample was measured 80 times as temperatures were increased in $50°$ C $\pm10°$ C increments up to $500°$ C, and at each temperature, the average interferogram was analyzed against the gold reference sample according to equation (3.1).

Spectral emissivity was measured at near-normal incidence ($10°$) to match the geometry of the Telops IFTS rear-surface view angle during the laser damage tests. Data from 2-12 μm was collected with a spectral resolution of $4\,cm^{-1}$. The spectral range of the Telops IFTS is $1.5 - 5.5\,\mu$m, so results will be shown in detail in the $2 - 5\,\mu$m band to illustrate the spectral emissivity values used to fit with collected spectral radiance data.

4.1.1 Matte Black Rear-Surface Paint.

The matte black paint found on the back surface of the laser-damage test samples was of primary importance in the creation of this database, since it was the only paint directly

viewed with a Telops IFTS. The paint in question was Stove Bright high temperature aerosol paint, made by Forest Technical Coatings. Under heating in the SOC-100, the samples themselves appeared to undergo little visible change, which is expected as the paint is advertised as a high-temperature stove paint made for extended use up to 650° C. The matte black rear-surface paint's temperature-evolving spectral emissivity is shown in Figure 4.1. A detailed view of the MWIR spectral region, for which the emissivity data is useful to the Telops IFTS radiance data, is shown in Figure 4.2.
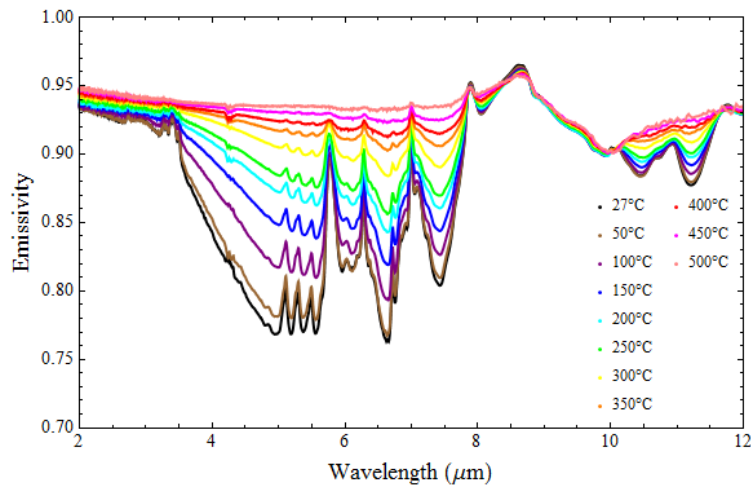
Figure 4.1: Temperature-dependent spectral emissivity for black painted Al2024-T3 alloy as temperature is increased from room temperature to 500° C.
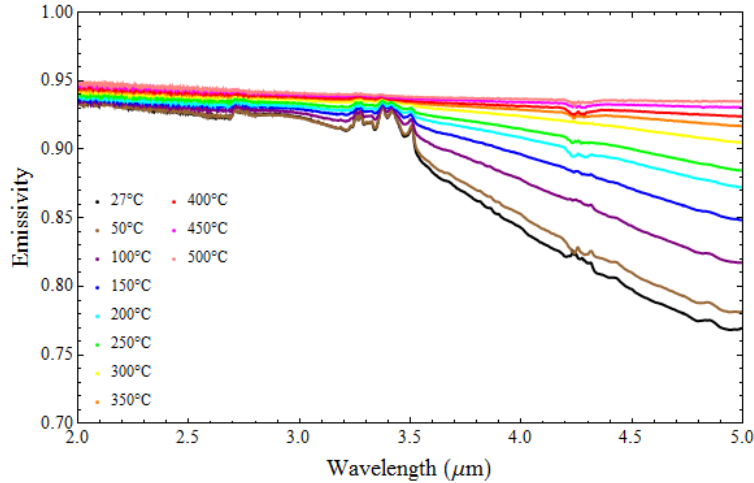
Figure 4.2: Detail of the spectral emissivity profiles for black painted Al2024-T3 alloy in the spectral sensitivity range of the Telops IFTS.

Though the paint did not appear to undergo visible change after heating, as shown in Figure 4.3, spectral emissivities were measured after the sample had been heated to 500° C to determine if the coating undergoes a physical change after being heated. Figure 4.4 shows the paint's dependence on its past heating. The paint's spectral emissivity was also tested after a second heating. This change was not significant compared to that from the first sample heating. Still, it is important to note that the matte black paint will have different spectral characteristics depending on whether or not it has been previously exposed to high temperatures.

Figure 4.3: Photograph of two different matte black painted samples, (left) before heating, and (right) after heating.

24
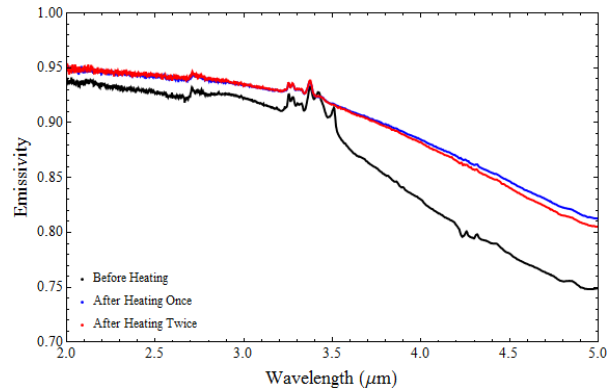
Figure 4.4: Spectral emissivity of one matte black painted aluminum sample before heating, after heating to 500° C once, and after heating to 500° C twice.

4.1.2 Camouflage Gray Front-Surface Paint.

Although the rear surface was the only one imaged by the Telops IFTS during the most recent laser damage tests, it is of interest to study the temperature-dependent emissivities of front surface coatings for future tests in which IFTS data may be collected from the front surface. As such, light gray camouflage aircraft paint was studied. Its temperature-evolving spectral emissivity is shown in Figure 4.5 over the full $2 - 12\,\mu$m band. Additionally, a detailed view of the spectral emissivities in the MWIR is shown in Figure 4.6
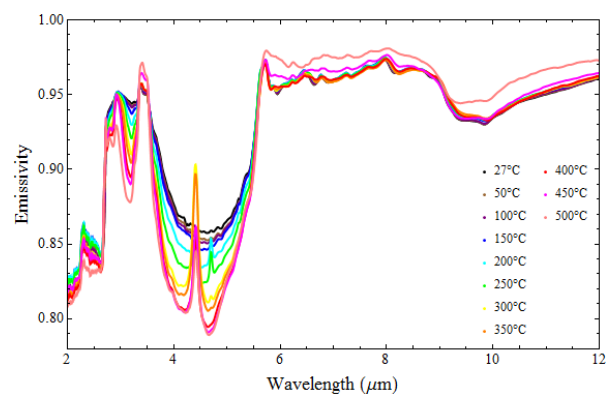
Figure 4.5: Spectral emissivity profiles for light gray camouflage painted Al2024-T3 alloy as temperature is increased from room temperature to 500° C.
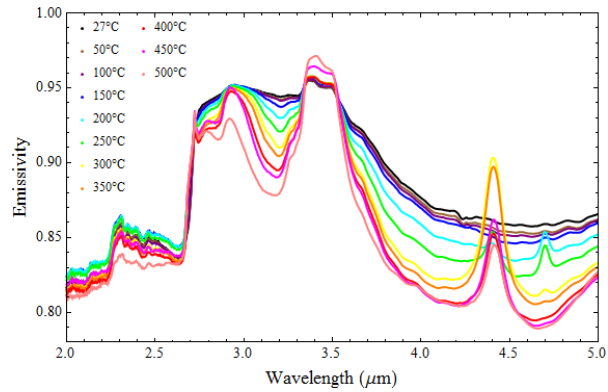
Figure 4.6: Spectral emissivity profiles for light gray camouflage painted Al2024-T3 alloy, in the spectral range of the Telops IFTS.

These light gray camouflage paint samples visually degraded in the SOC-100, as seen in Figure 4.7, after being heated to 500° C. The paint's change in spectral emissivity after heating is shown in Figure 4.8. This paint charring on the front surface of laser damage test samples is a well-documented phenomenon. [2] The paint degradation process can be seen in Figure 4.6, where there are peaks in emissivity at 4.4 and 4.7 μm as the samples are heated. Outgassing of organic volatiles is the likely cause of these features.
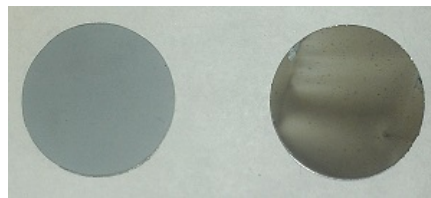
Figure 4.7: Image of light gray camouflage painted samples, (left) before heating, and (right) after heating. Streaking patterns are caused by the nitrogen purge gas flowing over the sample surface.
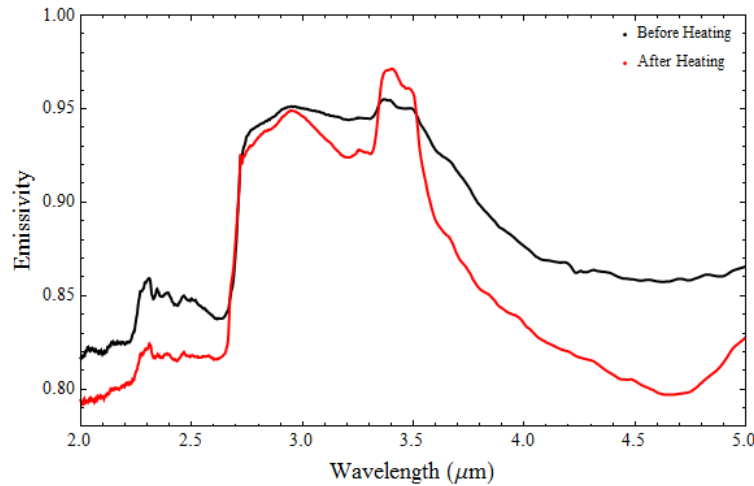
Figure 4.8: Spectral emissivity of a light gray camouflage painted aluminum sample before and after heating to 500° C, in the spectral range of the Telops IFTS.

4.1.3 Bare Aluminum Alloy.

Finally, temperature-evolving spectral emissivities were collected for bare Al2024-T3 samples. While high energy laser engagements will likely not occur on these samples, similarities were found between the collected emissivity spectra, shown in Figure 4.9, and established spectral emissivities in the literature. [15] In both cases, spectral emissivities had weak wavelength and temperature dependence in the MWIR and LWIR, and held average values of 0.04. In the case that paint is removed via ablation or shear wind flow, this data may provide more insight into the true temperature of a laser damage test sample.
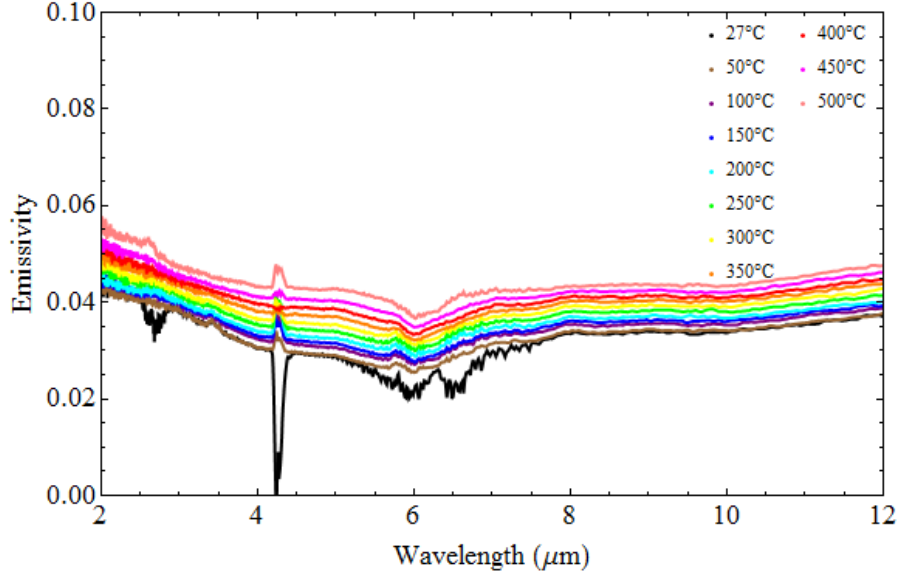
Figure 4.9: Temperature-dependent, spectral emissivity of bare Al2024-T3 alloy as temperature is increased from room temperature to 500° C.

4.2   Emissivity Database Application to Laser Damage Test Results

Laser damage tests conducted in July 2012 at the LHMEL facility employed a Telops IFTS observing the back surface of the samples. The time-dependent spectral radiance, measured at each pixel, was then used to extract temperature data at the corresponding pixel location by solving equation (4.1), where τ_{atm} is atmospheric transmission (calculated in a line-by-line radiative transfer model (LBLRTM) from the HITRAN database), and $ILS(\lambda' - \lambda)$ is the Telops instrument line shape function. The temperature is allowed to float within the blackbody radiance function, $L_{bb}(\lambda, T)$, until a best fit is found for the collected spectral radiance.

$$L(\lambda) = \int \tau_{atm}(\lambda)\epsilon(\lambda)L_{bb}(\lambda, T)ILS(\lambda' - \lambda)d\lambda \qquad (4.1)$$

All temperature estimations were made by Dr. Cameron Keenan at AFIT. An example of these temperature estimation methods is shown in Figure 4.10. The collected spectrum

was taken from a single pixel on the back surface of a laser damage test sample, after the burn-through hole had formed and reached its maximum size. At maximum burn-through hole size, the sample begins to approach a steady temperature. The pixel in question was far from the burn-through hole, where the sample temperature was assumed not to approach the melting point of Al2024-T3 (638° C). The blue data points represent the spectral radiance data collected from the Telops IFTS. The black trace represents the best fit for spectral radiance when a constant, graybody emissivity is assumed for the back-surface paint. The green trace represents the best fit for spectral radiance when the sample's emissivity is dictated by the temperature-dependent spectral emissivity database. Finally, the red trace shows an idealized blackbody spectral radiance curve at the best-fit temperature predicted using the emissivity database.
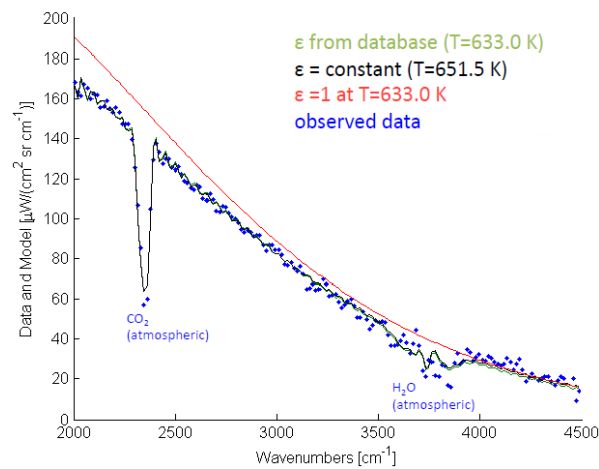
Figure 4.10: Spectral radiance measurement, and fitted spectral radiance results, of one pixel on the back surface of a painted metal sample, far from laser burn-through hole.

As expected, the spectral radiance from the ideal blackbody lies above all other traces. However, the best-fit lines for the two assumed spectral emissivities are more difficult to separate. It should be noted that the temperature predicted using a graybody assumption

29

(378.5° C) is 18.5° C higher than the temperature predicted by employing the spectral emissivity database (360.5° C). A more detailed investigation of the relative accuracy of each temperature estimation method follows.

4.2.1 Advantages of Direct Emissivity Measurements.

A comparison of the accuracy of the two temperature estimation methods discussed in the previous section is shown through a complete laser damage test in Figure 4.11, at the same pixel far from the burn-through hole discussed in the previous section. At $t \approx 2.5s$, the laser is turned on. Temperature increases rapidly until a burn-through hole begins to form at $t \approx 7s$. As the hole widens, less laser energy is incident on the test sample. At $t \approx 10s$, the hole has reached its maximum size and no more heat is being added to the system. At $t \approx 15s$, the laser is turned off and the sample cools again. In both figures, the IFTS was calibrated such that its noise-equivalent temperature (NET) was 270° C, so as temperature values approach this lower limit, the uncertainty shown in the error bars increases.
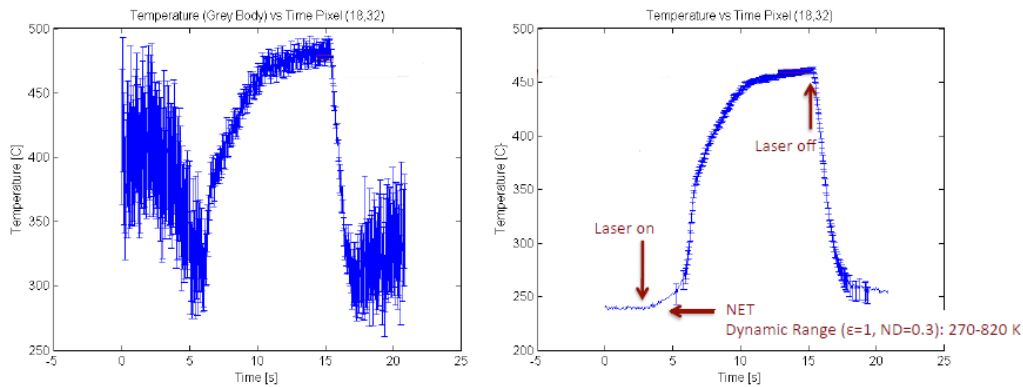
Figure 4.11: Comparison of temperature estimation accuracy during a laser damage test, from a pixel far away from the burn-through hole, assuming graybody emissivity (left) with that from incorporating the spectral emissivity database (right).

30

The best-fit temperature, as predicted using a graybody assumption for the back-surface paint, peaked at 475° C, with an uncertainty of ±25° C at that point in time as determined by the quality of the spectral radiance fit. In comparison, the best-fit temperature predicted using the emissivity database peaked at 455° C, with an uncertainty of ±5° C at that point in time. Here, it has been illustrated that away from the laser burn-through hole, where the sample temperatures achieved during the laser damage tests do not exceed the maximum achievable in the SOC-100, the emissivity database provides significantly more accurate temperature estimations.

4.2.2 Limits of Emissivity Data.

The temperature-dependent spectral emissivity database works well in estimating laser damage test sample temperatures when the temperature never exceeds the maximum achievable temperature of the SOC-100. However, temperatures on the samples in laser damage tests do exceed the database values close to the beam as the samples begin to melt. When the emissivity database is applied to a pixel directly adjacent to the burn-through hole, its spectral fit becomes poor as the sample reaches high temperatures, as shown in Figure 4.12. In this case, the graybody assumption fits the data noticeably closer than does the emissivity database. A number of hypotheses have been presented as to why this takes place, either that the paint rapidly degrades, or is removed as the alloy substrate underneath it begins melting.

When the temperature estimation uncertainties are viewed through the duration of a laser damage test, as in Figure 4.13, the database failure becomes apparent in that the best-fit error for temperature rapidly increases well beyond its expected error of ±5° C.

31
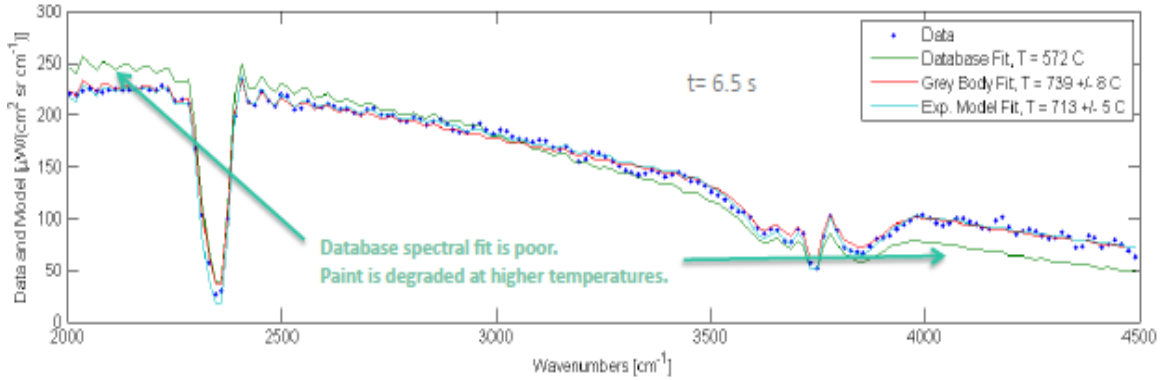
Figure 4.12: Spectral fit of Telops IFTS data at a pixel near the sample hole, after hole has opened. Blue dots represent collected spectral radiance from IFTS, the red curve represents the best spectral fit with assumed graybody emissivity, and the green curve represents the best spectral fit using the collected spectral emissivity values.
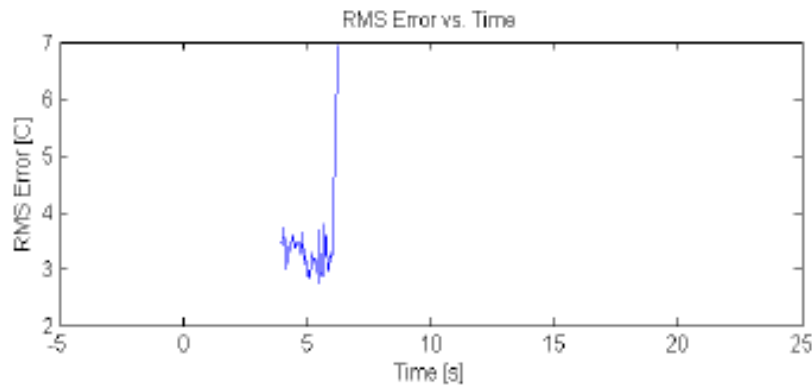
Figure 4.13: Time-evolving RMS error for best-fit temperature estimation using the emissivity database. Data is cut off when uncertainty exceeds the uncertainty resulting from graybody temperature estimates.

32

4.3 Summary

The temperature-dependent spectral emissivity database developed here has offered a significant improvement in temperature estimation accuracy in certain areas. Where the sample temperature during a laser damage test does not exceed the maximum achievable temperature of the SOC-100 measurements, spectral fits are strong, and uncertainties have been reduced from $\pm 25°$ C to $\pm 5°$ C. However, the failure of the measured emissivities to accurately predict temperature for pixels on or near the beam show the need for an alternate method to measure emissivities up to melt temperature, which will be discussed in Chapter V.

V. Experimental Method: Laser Reflectometer

The upper temperature limits of the spectral emissivity database necessitated the development of a new method for quickly measuring temperature-dependent reflectance of a laser damage test sample from room temperature to melt temperature. The method proposed and tested here is a laser reflectance probe, which will measure reflectance at a single wavelength, on a single spot on the sample. The methods are detailed in the following sections.

5.1 Mid-Wave Infrared Laser Source

The laser probe in use for this test is a Daylight Solutions Unicorn II quantum cascade laser operating at 3.77 μm. According to the laser specifications sheet [16], the beam's output power was rated at 67 mW, and was measured at 61 mW by a Thorlabs PM100 bolometer. The beam has a waist of 2.5 mm and a divergence of < 5 mrad.

5.2 Reflectance Collection Apparatus

A diagram outlining the different components of this experiment is found in Figure 5.1. The 3.77 μm laser was modulated via mechanical chopper at 650 Hz ±5 Hz. A small portion of the beam (7 mW) was then sampled by reflection from a pellicle beamsplitter and measured with a Cincinnati Electronics SNN-32I0 Indium Antimonide (InSb) detector paired with a built in transimpedence preamplifier with a response time of 70 ns. This reference arm was used to normalize the test data for any fluctuations in laser power during the course of the test.

The remaining beam (54 mW) was transmitted through the pellicle beamsplitter and incident on the temperature-controlled sample stage. In this experiment, 3" by 3" Al2024-T3 alloy samples were coated with the same high-temperature matte black paint as used during the laser damage tests, and during the SOC-100 temperature-dependent

34

spectral emissivity tests. The samples were heated via eight Watlow Firerod model C2A5 resistive cartridge heaters inserted into a copper backing plate in the sample stage. Temperature was controlled via Watlow Series 96 Proportional-integral-derivative (PID) temperature controller, with a thermocouple reading the sample's back-surface temperature for feedback. Laser light reflected off the heated sample surface was then collected by a Teledyne Judson J10D-M204-R02M InSb photovoltaic detector, paired with a Judson PA-9 preamplifier, which yielded a response time of 50 μs. During some tests, a $3.5 - 4\,\mu$m spectral filter was introduced to limit thermal background as the sample was heated close to melting temperature. Again, samples were heated in $50°$ C increments, this time with the upper limit placed at the melt temperature of the alloy, $638°$ C.
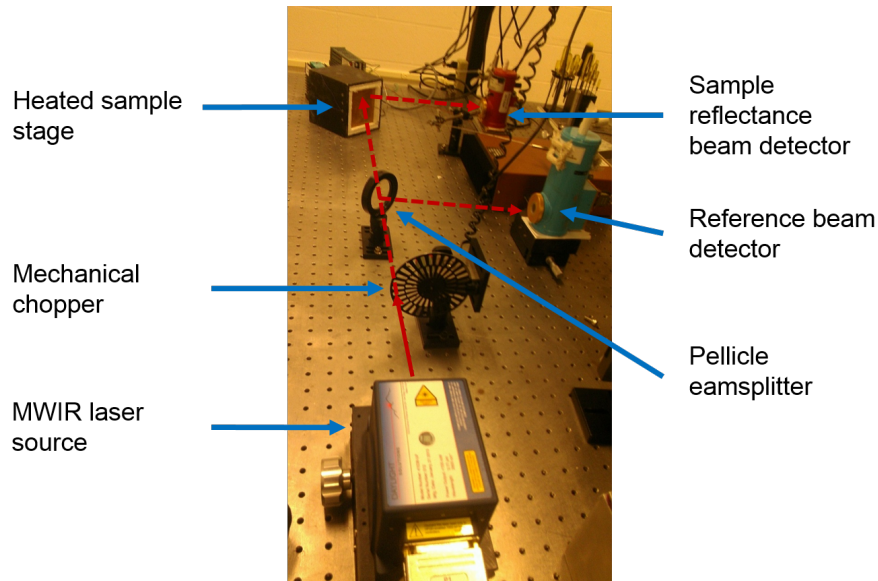
Figure 5.1: Detail of laser source, mechanical chopper, pellicle beamsplitter and reference detector.

5.3 Data Recording via Lock-In Amplifiers

Signals from the detectors were read by two Stanford Research Systems SR830 lock-in amplifiers. Here, the mechanical chopper frequency was used as the lock-in reference, and was compared against the reference and signal arms of the apparatus, respectively. 1,000 data points were collected at a sampling rate of 256 Hz and a time constant of 3 ms. The DC output signals from the lock-ins were sent to a computer via GPIB interface and analyzed in MATLAB.

5.4 Exploration of Different Test Geometries

The goal of this experiment was to create an *in situ* single-wavelength emissivity measurement technique, inferred from the fractional reflectance measurement, that can collect data rapidly throughout an entire laser damage test. A variety of test geometries was studied. Both specular and diffuse reflectance measurements were considered at a variety of incident and reflected angles. Additionally, an off-axis parabolic mirror (OAP) with a 6-inch effective focal length was introduced to determine the feasibility of imaging a point on the sample onto the detector from a larger solid angle, rather than simply collecting the reflectance within the solid angle subtended by the detector. This was done in order to test whether the specularity of the reflected beam was changing significantly during heating. The results, as well as a discussion, are presented in Chapter VI.

36

In this chapter, the results of the laser reflectometer experiment are discussed. First, the SOC-100 temperature-dependent emissivity data is converted to its fraction-of-room-temperature-value form for comparison to laser reflectance probe data. Next, an analysis of the method's sensitivity to errors in measured fractional reflectance is presented in order to validate the method as a legitimate tool for estimating temperatures during laser damage tests. Finally, the results of the laser reflectance probe experiment are presented, along with the challenges associated with each of the test geometries.

6.1   Calculation of Fractional Reflectance and Emissivity

Data points of overall signal magnitude from each lock-in amplifier were collected synchronously at a rate of 256 Hz. The data points were generated by dividing the total test signal by the reference signal at each synchronized point. This accounted for any variations in intensity from the laser source. Data points at each temperature were then averaged over all 1,000 collected points to find a final signal for each temperature, expressed as

$$V(T) = \frac{\sum_{i=1}^{1000} \frac{R_{test,i}}{R_{ref,i}}}{1000}. \tag{6.1}$$

After each data point was averaged, the signals were then normalized to the signal at room temperature, such that each subsequent signal would be interpreted as a fraction of the initial, room temperature (RT) signal. Equation (6.2) shows this relationship and its application to the change in reflectance of the sample.

$$\frac{V(T)}{V(RT)} = \frac{\rho_{3.77}(T)}{\rho_{3.77}(RT)} = \rho_{frac}(T) \tag{6.2}$$

The fractional reflectances are then converted back to emissivity as shown in

$$\epsilon_{3.77}(T) = 1 - \left[\rho_{frac}(T) \cdot \rho_{3.77}(RT) \right]. \tag{6.3}$$

37

6.2 SOC-100 Data as Fractional Reflectance Values

The reference against which the experimental data will be measured is the temperature-dependent emissivity from the SOC-100 measurements at the laser wavelength (3.77 μm). Figure 6.1 shows this data, from the high-temperature matte black paint found on the back surface of the laser damage testing target samples. Temperatures shown were recorded by the thermocouple in contact with the sample surface in the SOC-100 heating stage.
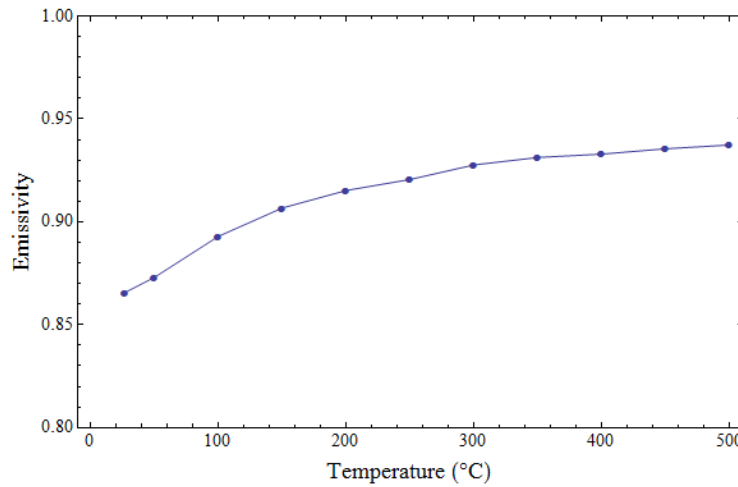

Figure 6.1: Temperature-dependent emissivity, measured by SOC-100, of high-temperature matte black painted samples at 3.77 μm.

Now, with a known temperature-dependent emissivity, it is possible to solve equation (6.3) for $\rho_{frac}(T)$ at every data point from the SOC-100. Figure 6.2 shows the reference data that will determine the accuracy of the results.

38
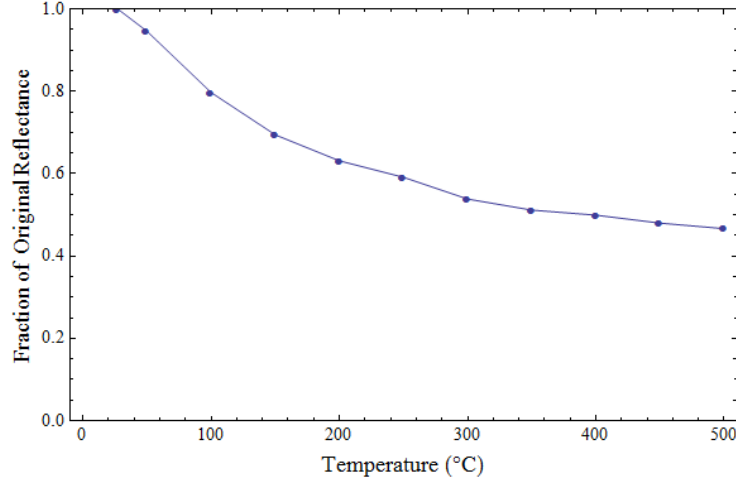
Figure 6.2: Fractional reflectance values for painted aluminum samples from SOC-100 data.

6.3 Fractional Reflectance and Temperature Uncertainty

As the goal of this experiment is to determine the feasibility of this laser reflectance probe to create reliable temperature estimates, it is important to consider the effects of measurement errors on predicted temperatures. Recalling Equation (2.15), which shows the relationship between predicted temperature and single-wavelength values for emissivity and spectral radiance, Equation (6.4) shows the change in estimated temperature with respect to emissivity.

$$\frac{\partial T}{\partial \epsilon} = -\frac{2h^2c^3}{k\lambda_0^6 L_\lambda(T)\left(\frac{2hc^2\epsilon}{\lambda^5 L_\lambda(T)} + 1\right)\ln\left[\frac{2hc^2\epsilon}{\lambda_0^5 L_\lambda(T)}\right]^2} \tag{6.4}$$

The change in temperature with respect to a change in emissivity can also be written as shown in Equation (6.5), which is an estimate valid for small values of $\Delta\epsilon$.

$$T + \Delta T = \frac{hc}{k\lambda_0 \ln\left[\frac{2hc^2(\epsilon_\lambda(T)+\Delta\epsilon)}{\lambda_0^5 L_\lambda(T)} + 1\right]} \tag{6.5}$$

Furthermore, when Equation (6.3) is substituted into the single-wavelength temperature estimate and the corresponding uncertainty term is introduced, its influence on estimated

39

temperature is described in

$$T + \Delta T = \frac{hc}{k\lambda_0 \ln\left[\frac{2hc^2\left(1-\left[\left(\rho_{frac}(T)+\Delta\rho_{frac}\right)\cdot\rho_{RT}\right]\right)}{\lambda_0^5 L_\lambda(T)} + 1\right]}.$$ (6.6)

Additionally, Equation (6.6) can be solved for estimated temperature error, ΔT, as a function of fractional reflectance error ($\Delta\rho_{frac}$) and true temperature (T), where

$$\Delta T(\Delta\rho_{frac}, T) = \frac{hc}{k\lambda_0 \ln\left[\frac{2hc^2\left(1-\left[\left(\rho_{frac}(T)+\Delta\rho_{frac}\right)\cdot\rho_{RT}\right]\right)}{\lambda_0^5 L_\lambda(T)} + 1\right]} - T.$$ (6.7)

For a complete picture of how errors in fractional reflectance impact the accuracy of temperature estimations, it is helpful to view a contour plot, as shown in Figure 6.3. Here, the accuracy of the estimated temperature is shown across a range of true sample temperatures (from room temperature to the melting point of Al2024-T3), and a wide range of possible errors in fractional reflectance values. For the purposes of this analysis, true temperature and collected spectral radiance are calculated from SOC-100 temperature-dependent emissivity data. It can be seen that as temperature is increased, estimate uncertainties become more severe. Still, at very close to the sample melt temperature, a fractional reflectance error of ±0.2 corresponds to an estimated temperature uncertainty of 7° C. It should be noted, however, that these uncertainty values are highly dependent on the initial emissivity values, and its temperature dependence. In this case, the high-temperature matte black paint showed a consistently low reflectance. A more reflective paint, on the other hand, would yield more pronounced uncertainties at near-melting temperature.

40
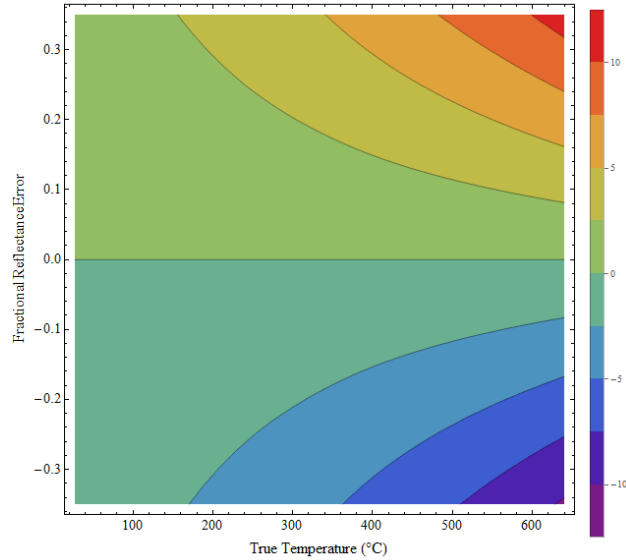
Figure 6.3: Uncertainty in estimated temperature values, as true temperature increases and fractional reflectance uncertainties are varied.

6.4   Results

A variety of detector geometries was tested for their accuracy and reliability. The following sections detail the geometries in the order they were studied.

6.4.1   Direct View.

The first detector geometry attempted was a direct view of the heated sample, with both specular and diffuse reflectances being investigated. The first test, shown in Figure 6.4, was conducted with the probe beam incident on the sample at 45°, and the specular reflectance measured directly, with the detector at 45°. The second test, shown in Figure 6.5, was conducted to measure diffuse reflectance from the sample, with the beam normally incident on the sample and the detector at 45° from normal.

41

Figure 6.4: Temperature-dependent fractional reflectance of a high-temperature matte black painted sample, with beam incident at 45° and specular reflectance measured with detector at 45°.

Figure 6.5: Temperature-dependent fractional reflectance of a high-temperature matte black painted sample, with beam normally incident and reflectance measured with detector at 45°.

Up until approximately $240 - 300°C$, both tests showed a similar downward trend to the SOC-100 reference. The diffuse reflectance case (with beam normally incident, detector looking at 45°) showed a closer correlation with fractional reflectance errors of ≈ 0.07. However, in both cases a sudden, catastrophic drop in signal occurred. Two

42

possibilities were considered as reasons for the signal loss. The first was that there was some change in surface conditions that caused a true signal loss due to changing reflectance characteristics. The second was that the integrated thermal power from the heated sample was saturating the detector with enough DC signal that the AC reflectance probe could no longer be clearly distinguished from the noise. These possibilities are addressed in the following two sections.

6.4.2 With Off-Axis Parabolic Mirror.

The possibility of signal loss due to surface composition or reflectance changes was evaluated by introducing a 3"-diameter OAP mirror to collect a larger reflected solid angle from the sample. The same two incident-reflected light geometries were considered. Figure 6.6 shows the fractional reflectance values where the laser probe was incident on the sample at 45°, and the OAP placed at 45°. Likewise, Figure 6.7 shows the fractional reflectance values recorded with the beam normally incident and probe at 45°.
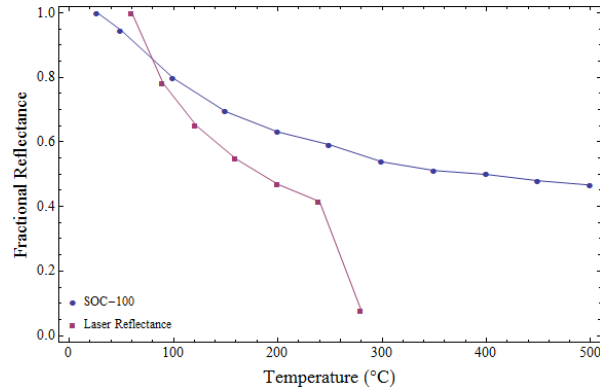

Figure 6.6: Temperature-dependent fractional reflectance of a high-temperature matte black painted sample, with beam incident at 45° and specular reflectance collected by an OAP mirror at 45° and measured by the detector in the OAP's image plane.
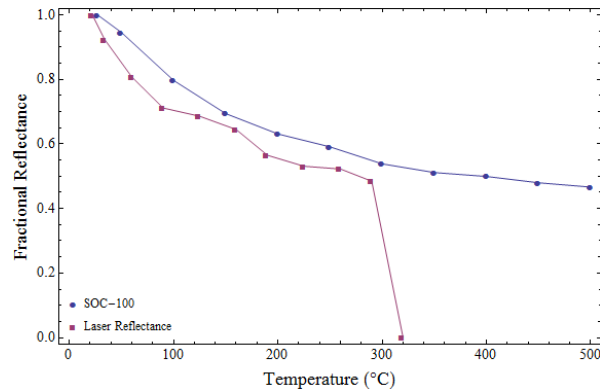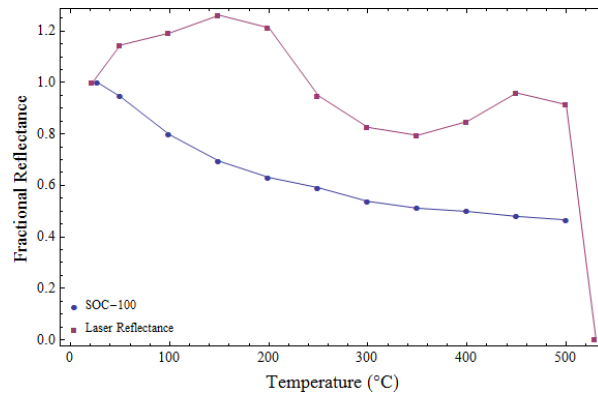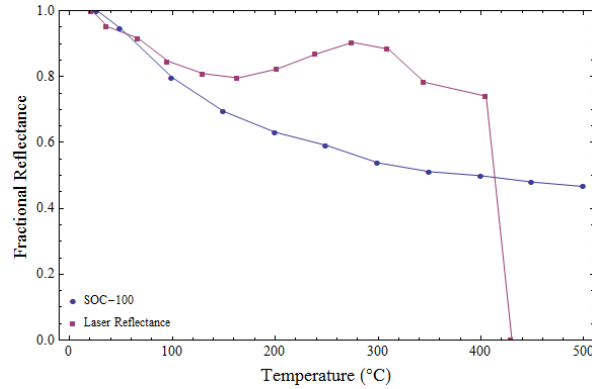
Figure 6.7: Temperature-dependent fractional reflectance of a high-temperature matte black painted sample, with beam normally incident and diffuse reflectance collected by an OAP mirror at 45° and measured by the detector in the OAP's image plane.

As is illustrated in Figures 6.6 and 6.7, the OAP caused a decrease in the reliability of the data in relation to the SOC-100 reference. Additionally, the signal drop-off still occurred, though at higher temperatures. The most likely reason for this improvement is that because the OAP images a smaller spot on the surface, there is less total thermal energy incident on the detector. These results indicated that the introduction of an OAP to image the beam spot on the sample was not effective at generating accurate results within the temperature range, or at keeping a steady signal from room temperature to sample melt temperature.

6.4.3 Direct View with Spectral Filter.

The possibility of DC saturation of the detector from thermal radiance was then addressed by returning to the direct-view arrangement, but with the introduction of a spectral filter transmissive between $3.5-4.0\,\mu$m, placed immediately in front of the detector. This way, total integrated power collected by the detector would be reduced and the AC laser probe would still be discernible from the thermal emission of the sample.

44

The first test geometry in which the spectral filter was employed was for the specular reflectance case, with the beam incident on the sample at 45° and the detector directly looking at the sample from 45°. Figures 6.8a and 6.8b show two tests, on different samples, using the same geometry.

(a) Test 1   (b) Test 2
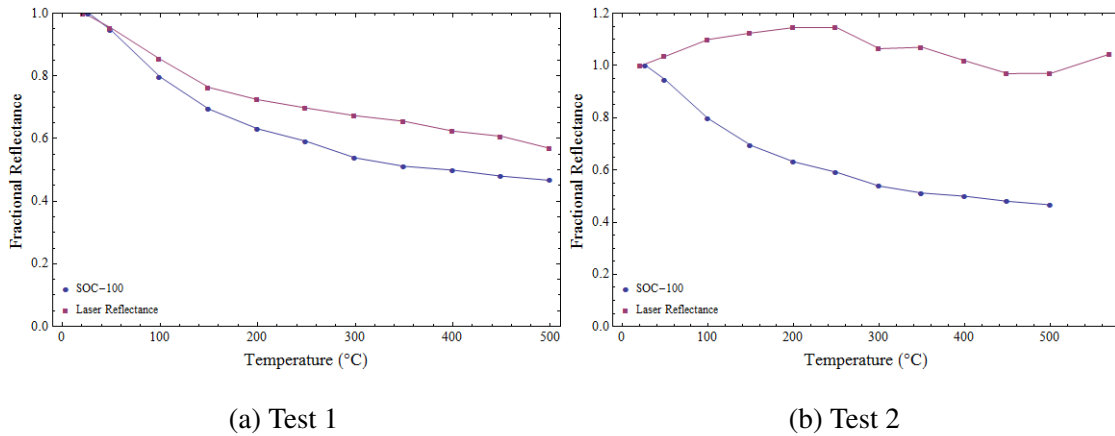
Figure 6.8: Two temperature scans, of two different samples, using a direct view of the sample through a spectral filter. Both tests were viewed in the specular case at 45°.

Of note is that the signal drop-off has been eliminated, enabling fractional reflectance measurements to be made up to the sample melt temperatures. This validates the earlier hypothesis that signal loss was due to detector saturation, and that the spectral filter reduced the total thermal energy incident on the detector enough for the modulated probe beam to be detected. However, as illustrated in Figures 6.8a and 6.8b, there are issues with experiment repeatability. In the case of Test 1, where the maximum difference between reference and test fractional reflectances was 0.12 at 500° C, a temperature uncertainty of 3.6°C can be expected, from Equation (6.7). However, in Test 2 where the fractional reflectance values are off by up to 0.5, temperature estimation uncertainties can reach 16° C.

6.5 Summary

The method of using a laser reflectance probe to accurately estimate temperatures on laser damage test samples has proven to be problematic. Issues encountered during the experiment included the AC laser probe signal being lost under the DC thermal radiance from the source at elevated temperatures, difficulty getting the beam spot to image onto the detector via the OAP mirror, and a lack of repeatability. Figures 6.5 and 6.8a provide an indication that reliable data may be gained from this method, but more testing will be required for the laser reflectance probe method to be validated.

VII. Conclusions and Recommendations

7.1 Main Findings

The first objective of this research was to create a database of temperature-dependent spectral emissivities for a variety of paint-substrate combinations. To this end, an SOC-100 HDR was employed to make the measurements. This instrument was able to provide accurate, repeatable results from room temperature to 500°C across a wide spectral range in the infrared. Spectra were collected for a typical Air Force camouflage gray paint, bare Al2024-T3 alloy, and for a high-temperature matte black paint used to coat rear surfaces of laser damage test samples in previous laser damage tests. Emissivity data from the matte black paint was then incorporated into an algorithm to estimate a surface temperature from the collected spectral radiance during the previous laser damage tests. In cases where the laser damage test samples did not exceed the maximum temperatures of the SOC-100 data, the estimates generated from the spectral emissivity data were shown to be more accurate than those in which the paint was assumed to behave as a graybody emitter. However, very close to the laser burn-through hole, as temperatures approached the melting point of the alloy, the spectral emissivity data became insufficient to accurately estimate temperature due to a lack of data above 500° C.

These limitations led to the second objective of the research, which was to develop a new method for evaluating emissivity at a single wavelength, able to be used during future laser damage tests. A laser probe, operating at a wavelength of 3.77 μm, was chosen so that a single-wavelength emissivity could be evaluated within the spectral range of the Telops IFTS, used to collect spectral radiance from laser damage test targets. Uncertainty analysis showed that the temperature estimates remain fairly stable (±10°C) with respect to fractional reflectance errors, but problems with the method remained. The first problem to be overcome was the saturation of the detector from thermal radiation of the test sample.

47

This was solved by placing a spectral filter in front of the detector, effectively cutting down the total thermal energy incident upon it from the sample. Still, questions remain about the robustness of this method, as results found from the same test geometries were not repeatable.

7.2   Recommendations for Future Research

The emissivity database is expected to work well far from the laser damage hole, but on the beam spot before burn-through, the rapidly-changing sample may be probed for reflectance with the laser reflectance methodology described here. The new method shows some promise in estimating temperatures, but more work needs to be done before it becomes feasible. Specifically:

- Ensure that the electrical load required to resistively heat the sample are not interfering with the detector pre-amplifiers or lock-in amplifiers.

- Employ a detector multiplexing technique such that the reference beam and test beam are incident on the same detector. This technique will reduce errors stemming from different detector gain and offsets.

- Find a particular incident-reflection geometry that yields reproducible results, and matches the referenced SOC-100 data.

- Use thinner test samples to reduce the amount of heat loss and increase the rate of temperature change on the samples. High energy lasers heat the samples rapidly, and the resistive cartridge heaters can only keep pace if the samples are made thin enough.

- Employ more advanced lock-in amplifiers to enable acquisition of time-stamped data.

- Perform absorptance measurements for front surface paints at laser wavelengths (1-2 μm) to aid in a predictive model for HEL weapon engagements.

48

7.3 Conclusions

The research presented here was done to improve the accuracy of temperature estimation in laser damage testing. It has been shown that employment of a database of temperature-dependent spectral emissivities significantly improves temperature estimations in areas where the sample does not exceed the maximum achievable temperature of the SOC-100 reflectometer. However, limits of the instrumentation prevent measurements of emissivity up to sample melt temperatures.

The second method for measuring the real-time reflectance for the purpose of measuring brightness temperature at a single wavelength has thus far proven to be problematic; thermal self-emission from the target sample necessitated spectral filtering to ensure enough signal at high temperatures to record fractional changes in reflectance. Additionally, results are highly dependent on the geometry of the incident and reflected beams, without very good reproducibility. Despite the problems, there remain some results that indicate this laser reflectance probe may be a viable method for temperature estimation. After addressing the recommendations above, it may be feasible to use the laser reflectance probe during future laser damage tests, so that a full picture of back-surface temperature evolution may be developed from beginning of HEL weapon engagement to burn-through.

49

Bibliography

[1] R. J. Harrach, "Analytical solutions for laser heating and burnthrough of opaque solid slabs," *Journal of Applied Physics*, vol. 48, no. 6, pp. 2370–2383, 1977.

[2] A. McLachlan and L. B. Whitbourn, "The coupling of continuous-wave laser radiation into painted aluminum-alloy plates," *Journal of Applied Physics*, vol. 53, no. 6, pp. 4038–4045, 1982.

[3] J. M. Palmer and B. G. Grant, *The Art of Radiometry*. Bellingham, WA: SPIE, 2010.

[4] A. Thompson, *Guide for the Use of the International System of Units (SI)*. National Institute of Standards and Technology, 2008.

[5] W. L. Wolfe and G. G. Zissis, *The Infrared Handbook*. Ann Arbor, MI: Infrared Information and Analysis Center, 1978.

[6] Surface Optics Corporation, San Diego, CA, *SOC-100 User's Guide*, June 2009.

[7] A. Lee and P. Norris, "A new optical method for measuring surface temperature at large incident probe abgles," *Review of Scientific Instruments*, vol. 68, pp. 1307–1311, 1997.

[8] S. D. W. Claeys and V. Quintard, "Laser probing of thermal behaviour of electronic components and its application in quality and reliability testing," *Microelectronic Engineering*, vol. 24, pp. 411–420, 1994.

[9] J. Longtin and C. Fan, "Laser-based temperature measurement at a liquid surface," in *Proceedings of 11th IHTC*, vol. 4, p. 119, 1998.

[10] T. Iuchi and S. Wada, "Simultaneous measurement of emissivity and temperature for glossy metals near room temperature," in *AIP Conference Proceedings*, vol. 684, p. 699, 2003.

[11] E. Dereniak and G. Boreman, *Infrared Detectors and Systems*. New York: Wiley, 1 ed., 1996.

[12] Stanford Research Systems, Sunnyvale, CA, *Model SR830 DSP Lock-In Amplifier User Manual*, 1993.

[13] M. Benson and M. Marciniak, "Design considerations regarding ellipsoidal mirror based reflectometers," *Optics Express*, vol. 21, no. 23, 2013.

[14] Thermo Electron Corporation, Madison, WI, *Nicolet 6700 FTIR User's Guide*, 2004.

[15] C. Wen and I. Mudawar, "Emissivity characteristics of roughened aluminum alloy surfaces and assessment of multispectral radiation thermometry (mrt) emissivity models," *International Journal of Heat and Mass Transfer*, vol. 47, pp. 3591–3605, 2004.

[16] Daylight Solutions, San Diego, CA, *Spec Sheet: Unicorn II Fixed-Wavelength Mid-IR External Cavity Lasers*.

REPORT DOCUMENTATION PAGE

Form Approved
OMB No. 0704–0188

1. REPORT DATE *(DD–MM–YYYY)*	2. REPORT TYPE	3. DATES COVERED *(From — To)*
27–03–2014	Master's Thesis	Jan 2012–Mar 2014

4. TITLE AND SUBTITLE

Direct Emissivity Measurements of Painted Metals
for Improved Temperature Estimation During
Laser Damage Testing

5a. CONTRACT NUMBER

5b. GRANT NUMBER

5c. PROGRAM ELEMENT NUMBER

6. AUTHOR(S)

Baumann, Sean M., Civilian

5d. PROJECT NUMBER

5e. TASK NUMBER

5f. WORK UNIT NUMBER

7. PERFORMING ORGANIZATION NAME(S) AND ADDRESS(ES)

Air Force Institute of Technology
Graduate School of Engineering and Management (AFIT/EN)
2950 Hobson Way
WPAFB, OH 45433-7765

8. PERFORMING ORGANIZATION REPORT NUMBER

AFIT-ENP-14-M-43

9. SPONSORING / MONITORING AGENCY NAME(S) AND ADDRESS(ES)

Harro Ackermann
High Energy Laser-Joint Technology Office
801 University Blvd SE, Suite 209
ALbuquerque, NM 87106
(505) 248-8208, harro.ackermann@jto.hpc.mil

10. SPONSOR/MONITOR'S ACRONYM(S)

HEL-JTO

11. SPONSOR/MONITOR'S REPORT NUMBER(S)

12. DISTRIBUTION / AVAILABILITY STATEMENT
DISTRIBUTION STATEMENT A:
APPROVED FOR PUBLIC RELEASE; DISTRIBUTION UNLIMITED

13. SUPPLEMENTARY NOTES
This work is declared a work of the U.S. Government and is not subject to copyright protection in the United States.

14. ABSTRACT

A database of spectral, temperature dependent emissivities was created for a range of painted aluminum laser damage testing targets with the purpose of improving accuracy in temperature estimates on front and back target surfaces during laser damage tests. Previous temperature estimations were made by fitting an assumed graybody radiance curve to the radiance measured from the back surface via a Telops imaging Fourier transform spectrometer. In this work, spectral emissivity measurements were made using an SOC-100 hemispherical directional reflectometer and Nicolet Fourier transform infrared spectrometer. Of particular interest was a high temperature matte black enamel paint used to coat the rear surfaces of the aluminum samples. Previously, the paint was assumed to have a spectrally flat and temperature-invariant emissivity. Collected data showed spectral variance and temperature dependence. Back-surface temperature estimations of laser damage test samples were improved from $\pm 25°$ C to $\pm 5°$ C away from the beam center. At beam center, temperatures exceeded the capabilities of the reflectometer, so a new method was developed using a mid-infrared laser probe to measure temperature dependent reflectance. The new method may be used in future laser damage tests to estimate single-wavelength temperatures up to the target melting point. Accurate temperature measurements in laser damage testing will be helpful in informing a predictive model for future high energy laser weapon engagements.

15. SUBJECT TERMS
laser lethality emissivity painted metals

16. SECURITY CLASSIFICATION OF:

a. REPORT	b. ABSTRACT	c. THIS PAGE	17. LIMITATION OF ABSTRACT	18. NUMBER OF PAGES	19a. NAME OF RESPONSIBLE PERSON
U	U	U	UU	68	Dr. Michael A. Marciniak (ENP)

19b. TELEPHONE NUMBER *(include area code)*
(937)255-3636 x4529; michael.marciniak@afit.edu

Standard Form 298 (Rev. 8–98)
Prescribed by ANSI Std. Z39.18